# Sparse Bayesian reconstruction method for multispectral bioluminescence tomography

**Jinchao Feng (冯金超)[1], Kebin Jia (贾克斌)[1], Chenghu Qin (秦承虎)[2], Shouping Zhu (朱守平)[2], Xin Yang (杨 鑫)[2], and Jie Tian (田 捷)[2,3*]**

[1] *College of Electronic Information and Control Engineering, Beijing University of Technology, Beijing 100124, China*

[2] *Medical Image Processing Group, Institute of Automation, Chinese Academy of Sciences, Beijing 100190, China*

[3] *Life Science Research Center, Xidian University, Xi'an 710071, China*

[*] *E-mail: tian@ieee.org*

Received March 1, 2010

We present a sparse Bayesian reconstruction method based on multiple types of *a priori* information for multispectral bioluminescence tomography (BLT). In the Bayesian approach, five kinds of *a priori* information are incorporated, reducing the ill-posedness of BLT. Specifically, source sparsity characteristic is considered to promote reconstruction results. Considering the computational burden in the multispectral case, a series of strategies is adopted to improve computational efficiency, such as optimal permissible source region strategy and node model of the finite element method. The performance of the proposed algorithm is validated by a heterogeneous three-dimensional (3D) micron scale computed tomography atlas and a mouse-shaped phantom. Reconstructed results demonstrate the feasibility and effectiveness of the proposed algorithm.

*OCIS codes:* 100.3010, 100.3190, 170.3010, 170.6960.

*doi: 10.3788/COL20100810.1010.*

The emergence of new imaging modalities and approaches that provide cellular and molecular information has led to the nascent field of molecular imaging. Methods based on detecting optical signals in a small animal have been leading this field[1,2]. The light-emitting enzymes, and the technologies for detecting their weak bioluminescent signals with a highly sensitive charge-coupled device (CCD) camera in living subjects, comprise the method called *in vivo* bioluminescence imaging[3].

Much effort has been devoted to transforming bioluminescence imaging from a planar imaging technique into a truly three-dimensional (3D) tomographic modality application to small animals, because planar bioluminescent imaging cannot provide depth information[3]. The resolution of planar bioluminescent imaging is also limited due to the nature of surface imaging. Therefore, bioluminescence tomography (BLT) is developed to explore depth information and enhance bioluminescence imaging resolution. As a result, BLT is particularly attractive for *in vivo* applications.

Generally, BLT is an ill-posed problem and the uniqueness of the BLT solution has been proven theoretically[4]. The uniqueness theory is not only instructional in reconstructing a bioluminescent source distribution, but also presents that the ill-posedness of BLT could be overcome with sufficient *a priori* information.

Since the concept of BLT was introduced, it has made great progress in modeling and reconstruction algorithms[5−11]. Currently, BLT reconstruction-based spectrum information has gained much attention as BLT reconstruction results have improved, with hyperspectral and multispectral methods[5−8]. In addition, the importance of multiple types of *a priori* information has been recognized. The more the *a priori* information one applies, the better the results obtained.

The Bayesian approach provides a framework to incorporate multiple types of *a priori* information. We have proposed a BLT reconstruction algorithm based on the Bayesian approach to reconstruct a bioluminescent source, in which a generalized adaptive Gaussian Markov random field (GGMRF) prior model for unknown source density estimation is presented[9]. However, the sparse nature of the internal source to promote reconstructed quality is not considered in the prior model[10]. Furthermore, the permissible source region used in the previous algorithm is inferred through the light power distribution on the surface, which is hardly determined when the underlying source is located in a deep position. The large-scale reconstruction data also significantly affect reconstructed efficiency in the multispectral case.

In this letter, we describe a sparse Bayesian approach for multispectral BLT. Furthermore, multiple types of *a priori* information are incorporated into the Bayesian framework to reduce the ill-posedness of the BLT problem, specifically the sparsity of source and the optimal permissible source region.

In bioluminescence imaging, photon propagation can be described by the steady-state diffusion equation and Robin boundary condition. Taking into account the influence of light wavelength $\lambda$ on tissue optical property, the following model is thus given:

$$-\nabla\cdot[D(\mathbf{r},\lambda)\nabla\Phi(\mathbf{r},\lambda)]+\mu_a(\mathbf{r},\lambda)\Phi(\mathbf{r},\lambda)=x(\mathbf{r},\lambda)\quad(\mathbf{r}\in\Omega),\tag{1}$$

$$\Phi(\mathbf{r},\lambda)+2A(\mathbf{r};n,n')D(\mathbf{r},\lambda)[\nu(\mathbf{r})\cdot\nabla\Phi(\mathbf{r},\lambda)]=0\quad(\mathbf{r}\in\partial\Omega),\tag{2}$$

where $\Omega$ is a bounded smooth domain; $\partial\Omega$ is the corresponding boundary; $\Phi(\mathbf{r},\lambda)$ denotes the photon flux

 

density ($\mathrm{W/mm^2}$); $x(\mathbf{r},\lambda)$ is the bioluminescent source density ($\mathrm{W/mm^3}$); $\mu_{\mathrm{a}}(\mathbf{r},\lambda)$ is the absorption coefficient ($\mathrm{mm^{-1}}$); $\mathrm{D}(\mathbf{r},\lambda)$ is the optical diffusion coefficient (mm) $g$ is the anisotropy parameter; and $\nu(\mathbf{r})$ is the unit outer normal on $\partial\Omega$. Given the mismatch between refractive indices $n$ for $\Omega$ and $n'$ for the external medium, $A(\mathbf{r};n,n')$ can be approximately represented as $A(\mathbf{r};n,n') \approx \frac{1+R(\mathbf{r})}{1-R(\mathbf{r})}$, where $R(\mathbf{r}) \approx -1.4339n^{-2} + 0.7099n^{-1} + 0.6681 + 0.0636n$. The measured quantity is the outgoing flux density $\mathrm{Q}(\mathbf{r},\lambda)$ on boundary $\partial\Omega$ and can be expressed as

$$\begin{aligned} Q(\mathbf{r},\lambda) &= -D(\mathbf{r},\lambda)(\nu(\mathbf{r})\cdot\nabla\Phi(\mathbf{r},\lambda)) \\ &= \frac{\Phi(\mathbf{r},\lambda)}{2A(\mathbf{r};n,n')} \quad (\mathbf{r}\in\partial\Omega). \end{aligned} \tag{3}$$

In the practical experiment, outgoing flux density is generally detected with a bandpass filter, thus the continuous spectral range of bioluminescence light can be divided into $m$ bands $\tau_1,\cdots,\tau_m$, with $\tau_l=[\lambda_{l-1},\lambda_l]$, $l=1,2,\cdots,m$. Calculating the multispectral forward model requires a solution for the monochromatic case for each wavelength $\tau_l$. Generally, a finite element method based on discretized elements is adopted. However, the computation burden is very large in the multispectral case. To improve reconstruction speed, the finite element method based on nodes is applied to compute the forward model for each wavelength $\tau_l$[12]. We use the vector $\mathbf{x}$ to denote the set of unknown source density. Finally, a vector function $f(\mathbf{x})$ is obtained by integrating the monochromatic models over the source spectrum[7−9].

The uniqueness theorem shows that the BLT is not unique unless adequate *a priori* information is incorporated[4]. In the algorithm, besides multispectral information, anatomical and optical information of tissues are first used to deal with the non-uniqueness of BLT and constrain the possible solution of source reconstruction. The importance of permissible source region strategy is widely applied[7−9,12]. In this letter, an optimal permissible source region strategy is applied to improve reconstruction quality[8]. In finite element analysis, the given domain $\Omega$ can be discretized into $N_{\mathrm{t}}$ tetrahedron elements and $N_{\mathrm{v}}$ vertex nodes. Taking into account the optimal permissible source region information PS, there are $N_{\mathrm{P}}$ independent vertices in the permissible source region which represent the possible unknown source distribution. Column vector $\mathbf{x}$ is then reduced to the set of source density distribution of $N_{\mathrm{P}}$ vertices.

$\Phi_k^{\mathrm{meas}}(\tau_l)$ $(l=1,\cdots,m)$ is assumed as the measured photon flux density of wavelength $\tau_l$ at the $k$th detector position $(k=1,2,\cdots,M)$. The measurements of wavelength $\tau_l$ as single column vectors $\mathbf{y}(\tau_l)$: $\mathbf{y}(\tau_l)=[\Phi_1^{\mathrm{meas}}(\tau_l),\Phi_2^{\mathrm{meas}}(\tau_l),\cdots,\Phi_M^{\mathrm{meas}}(\tau_l)]^{\mathrm{T}}$ are then organized. In the multispectral case, the measurements are organized as a vector $\mathbf{y}=[\mathbf{y}(\tau_1),\mathbf{y}(\tau_2),\cdots,\mathbf{y}(\tau_m)]^{\mathrm{T}}$. The maximum a *posteriori* (MAP) estimate of $\mathbf{x}$ given by the measurement vector $\mathbf{y}$ can be represented as

$$\begin{aligned} \hat{\mathbf{x}}_{\mathrm{MAP}} &= \arg\max_{\mathbf{x}\geq 0} \log p(\mathbf{x}|\mathbf{y}) \\ &= \arg\max_{\mathbf{x}\geq 0} \big\{\log p(\mathbf{y}|\mathbf{x}) + \log p(\mathbf{x})\big\}. \end{aligned} \tag{4}$$

Considering the real physical meaning, nonnegative constraint $\mathbf{x}\geq 0$ is adopted. Taking into account anatomical tissue information $\boldsymbol{C}$ and optimal permissible source region information $\mathbf{PS}$, the MAP estimate can be further modified as

$$\begin{aligned} \hat{\mathbf{x}}_{\mathrm{MAP}} = \arg\max_{\mathbf{x}\geq 0} \big\{ &\log p(\mathbf{y}|\mathbf{x},\boldsymbol{C},\mathbf{PS}) \\ &+ \log p(\mathbf{x}|\boldsymbol{C},\mathbf{PS})\big\}, \end{aligned} \tag{5}$$

where $p(\mathbf{y}|\mathbf{x},\boldsymbol{C},\mathbf{PS})$ is the data likelihood and $p(\mathbf{x}|\boldsymbol{C},\mathbf{PS})$ is the conditional probability density function of $\mathbf{x}$ given $\boldsymbol{C}$ and $\mathbf{PS}$. Given the forward model in Eqs. (1) and (2), the data likelihood is governed mainly by noise statistics. Therefore, Eq. (5) is reduced to

$$\hat{\mathbf{x}}_{\mathrm{MAP}} = \arg\max_{\mathbf{x}\geq 0} \big\{\log p(\mathbf{y}|\mathbf{x}) + \log p(\mathbf{x}|\boldsymbol{C},\mathbf{PS})\big\}. \tag{6}$$

In the Bayesian framework, the data likelihood $p(\mathbf{y}|\mathbf{x})$ is required. The bioluminescence experiment generally operates at low temperature, therefore photon detection can be modeled using shot noise statistics. Thus, the data likelihood can be given by[13]

$$p(\mathbf{y}|\mathbf{x}) = \frac{1}{(\pi\alpha)^{m*M}|\Lambda|^{-1}} \exp\left[-\frac{\|\mathbf{y}-f(\mathbf{x})\|_\Lambda^2}{\alpha}\right], \tag{7}$$

where $\alpha$ is the parameter related to noise variance, $\Lambda$ is the diagonal covariance matrix with the size of $(m*M)\times(m*M)$, $\|\omega\|_\Lambda^2=\omega^{\mathrm{T}}\Lambda\omega$, and the vector value function $f(\mathbf{x})$ represents the exact value of the outgoing flux for the assumed value of source density $\mathbf{x}$, which has been solved previously. For BLT, we assume that the measurements are statistically independent with the variance of each measurement equal to its mean[13], therefore $\Lambda$ is diagonal. In our simulations, we approximately assume $\Lambda$ as

$$\Lambda = \begin{bmatrix} \Phi_1^{\mathrm{meas}}(\tau_l) & \cdots & 0 & 0 & \cdots & 0 \\ \vdots & \ddots & \vdots & \vdots & & \vdots \\ 0 & \cdots & \Phi_M^{\mathrm{meas}}(\tau_l) & 0 & \cdots & 0 \\ 0 & \cdots & 0 & \Phi_1^{\mathrm{meas}}(\tau_2) & \cdots & 0 \\ \vdots & \cdots & \vdots & \vdots & \ddots & \vdots \\ 0 & \cdots & 0 & 0 & \cdots & \Phi_M^{\mathrm{meas}}(\tau_m) \end{bmatrix}. \tag{8}$$

Bayesian framework requires that a prior unknown variable $\mathbf{x}$ is assigned. Now, the importance of the sparseness of signal has been recently recognized, and the reconstruction results could benefit from the *a priori* information[10]. In the proposed algorithm, sparseness, which is the Laplace density function,

is used:

$$p(\mathbf{x}|\boldsymbol{C},\mathbf{PS}) = (\lambda_s/2)^N \exp\left(-\lambda \sum_{i=1}^{N} |x_i|\right), \tag{9}$$

where $\lambda_s$ denotes scale parameters, which could be determined by the algorithm proposed in Ref. [14]. If $\alpha$ is unknown, referring to Eqs. (7) and (8), the source reconstruction problem can be stated as the following optimization problem:

$$\arg\max_{\mathbf{x}\geq 0}\max_{\alpha}\left\{-\frac{1}{\alpha}\|\mathbf{y}-f(\mathbf{x})\|_{\Lambda}^2 - M*m*\log\alpha + N\log(\lambda/2) - \lambda\sum_{i=1}^{N}|x_i|\right\}. \tag{10}$$

In the optimization process, $\alpha$ is adaptively estimated, which can be solved by viewing the problem (9) as a cost function of $\alpha$ and setting the derivative with respect to $\alpha$ equal to zero. We can then obtain

$$\alpha = \frac{1}{M*m}\|\mathbf{y}-f(\mathbf{x})\|_{\Lambda}^2. \tag{11}$$

Substituting Eq. (10) into (9), the optimization problem is converted into

$$\hat{\mathbf{x}} = \arg\max_{\mathbf{x}\geq 0}\left\{-M*m - M*m*\log\left(\frac{1}{M*m}\|\mathbf{y}-f(\mathbf{x})\|_{\Lambda}^2\right) + N\log(\lambda/2) - \lambda\sum_{i=1}^{N}|x_i|\right\}, \tag{12}$$

where $\hat{\mathbf{x}}$ is an estimate of the unknown source density $\mathbf{x}$. After neglecting constant terms, we can define the log posterior probability $l(\mathbf{x})$ as

$$l(\mathbf{x}) = -M*m*\log\left(\frac{1}{M*m}\|\mathbf{y}-f(\mathbf{x})\|_{\Lambda}^2\right) - \lambda\sum_{i=1}^{N}|x_i|. \tag{13}$$

The log posterior probability in Eq. (12) is used as a criterion for the convergence in our experimental results. In the practical calculation procedure, maximizing $l(\mathbf{x})$ by maximizing with respect to $\alpha$ and $\mathbf{x}$ uses the following equations:

$$\hat{\alpha} = \frac{1}{M*m}\|\mathbf{y}-f(\hat{\mathbf{x}})\|_{\Lambda}^2, \tag{14}$$

$$\hat{\mathbf{x}} = \arg\max_{\mathbf{x}\geq 0}\left\{-\frac{1}{\hat{\alpha}}\|\mathbf{y}-f(\mathbf{x})\|_{\Lambda}^2 - \lambda\sum_{i=1}^{N}|x_i|\right\}. \tag{15}$$

In this letter, a 3D micron scale computed tomography (micro-CT) mouse atlas is used to provide anatomical information. The mouse is then manually segmented into different tissue organs. In the following bioluminescence experiments, only the thorax micro-CT images are used, including lung, bone, heart, liver, and muscle, as shown in Fig. 1. Based on the emission spectral distribution, the spectrum range of [600, 750] nm can be divided into three discrete bins with a step of 50 nm. In the experiments, the optical properties of each component are assumed to be *a priori* information and computed according to the formulations given in Ref. [15]. The results are compiled in Table 1.

In view of "inverse crime" of BLT, the synthetic data are produced using Monte-Carlo-based method[16]. The mesh used in this method includes 49992 triangles and 24998 surface measurement points.

To avoid the "inverse crime", the mesh used in the reconstruction procedure is a much coarser volumetric mesh than that used in the simulating photon transport, which includes 2579 nodes, 13200 tetrahedron elements, and 697 boundary measurement points. All reconstructions were performed on a computer with an Intel processor (Pentium 4, 3.4 GHz) and 2-GB RAM. The convergence criterion was $l_k(\mathbf{x}) - l_{k-1}(\mathbf{x}) < 0.02$ or $k > k_{\max}$, where $k$ is the iterative number and $k_{\max}$ is the maximum iterative number.

At first, a solid spherical source with 1-mm radius was centered at 22.8, 28.6, and 12.5 mm inside the lung. With the proposed algorithm, the reconstruction results are shown is Fig. 2. We can accurately localize the source and the center position of the reconstructed source at 23.48, 28.55, and 12.04 mm. The reconstructed time was about 240 s. Figure 3 shows the convergence of the log posterior probability as a function of the number of iterations, which reveals the fast convergence.

The parameters used in our algorithm were adaptively

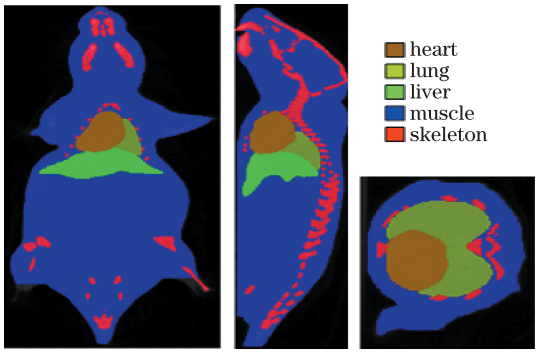


(a) (b) (c)

Fig. 1. View of the mouse phantom after segmenting. (a) Coronal view of micro-CT data; (b) sagittal view; (c) transverse view.

**Table 1. Optical Parameters in Different Bands ($mm^{-1}$)**

| Material | | Muscle | Heart | Lung | Liver | Bone |
|---|---|---|---|---|---|---|
| 600–650 nm | $\mu_a$ | 0.244 | 0.166 | 0.549 | 0.993 | 0.170 |
| | $\mu_s'$ | 0.527 | 1.069 | 2.259 | 0.731 | 2.775 |
| 660–700 nm | $\mu_a$ | 0.077 | 0.052 | 0.174 | 0.313 | 0.054 |
| | $\mu_s'$ | 0.413 | 0.945 | 2.157 | 0.668 | 2.444 |
| 700–750 nm | $\mu_a$ | 0.040 | 0.028 | 0.090 | 0.165 | 0.028 |
| | $\mu_s'$ | 0.337 | 0.853 | 2.077 | 0.620 | 2.201 |

estimated. To illustrate its feasibility, we compared it with the conventional sparse method, i.e., l1 regularization[10]. Similar reconstructed results with the conventional sparse method are shown in Fig. 4. The corresponding regularization parameter was $1.0 \times 10^{-9}$, which was chosen by experimental method. The reconstruction took about 960 s in the above mentioned computer.

Finally, a light source was placed almost at the center position of the CT mouse (at 20.8, 30.98, and 12.5 mm) to verify the proposed algorithm. The reconstructed results are demonstrated in Fig. 5. The source is shown to localize accurately (20.37, 31.05, and 12.95 mm). This accounts for the good source depth reconstruction of the proposed algorithm.

To verify the proposed algorithm, a commercially available solid mouse-shaped homogeneous phantom with an embedded bioluminescence source was used. More detailed information about the phantom can be found in Refs. [10, 17]. To acquire the phantom shape and the source position, a micro-CT system was used. The mesh with 1694 nodes and 6416 tetrahedral elements used for reconstruction was obtained based on the micro-CT images (Fig. 6(a)). To acquire spectral measurement data, a group of cutoff filters and a liquid-nitrogen-cooled back illuminated CCD camera were used. After image processing, we obtained two bands of measurement data, specifically [600, 650] nm and [650, 700] nm. The measured data

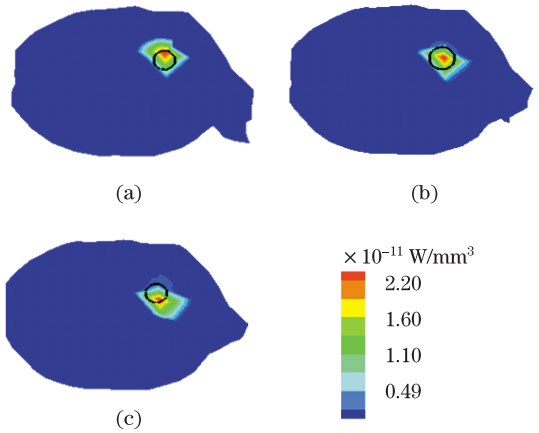


Fig. 2. Reconstructed light source distributions for three different slices of the reconstruction. (a) and (c) are perpendicular to the $z$-axis direction off the actual source's center at about $\mp$ 0.5 mm, (b) is through the actual source's center. The black circles denote the actual source.

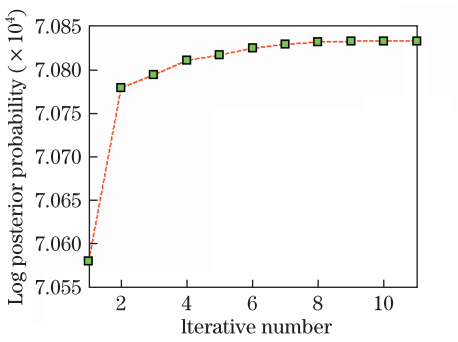


Fig. 3. Log posterior probability as a function of number of iterations.

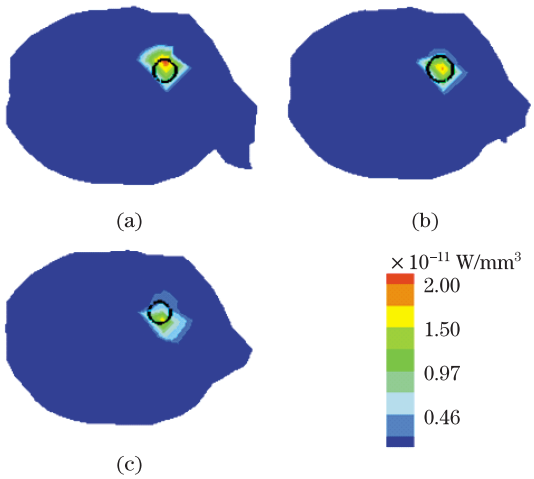


Fig. 4. Reconstructed light source distributions with 11 regularization for three slices of (a) $z = 12$ mm, (b) $z = 12.5$ mm, and (c) $z = 13$ mm, respectively.

were mapped on the surface of the phantom. Figure 6(b) illustrates the mapped result for the band [600, 650] nm. The corresponding optical parameters of these two bands and the energy contributions can be obtained by the product introduction. The actual source position (21.2, 25.3, and 28.4 mm) was also determined by micro-CT images.

When the BLT reconstruction was performed using the monochromatic experimental data in [600, 650] nm, the source was not localized with the proposed algorithm. The corresponding reconstructed result is shown in Fig. 7(a). However, a promising result was obtained with the proposed algorithm, and the reconstructed central position of the source was 21.6, 25.0, and 30.2 mm, as shown in Fig. 7(b). The reconstructed central position was 23.2, 27.2, and 27.8 mm with the method of Ref. [9]. The result is illustrated in Fig. 7(c). The reconstructed results revealed that our tomographic algorithm can provide high-performance reconstruction quality.

In this letter, a sparse Bayesian based reconstruction algorithm is proposed for multispectral BLT. Multiple types of *a priori* information are utilized to improve BLT reconstruction. Sparse source characteristics are also considered in the Bayesian approach. Related parameters used in the Bayesian approach are adaptively estimated, which makes the algorithm appropriate for practical application. Simulation verifications with Monte-Carlo-based data demonstrate that our proposed algorithm can acquire similar reconstructed results with the popular l1 sparsity regularization. Reconstruction of sources localized at deeper positions further proves the effectiveness of the proposed algorithm. In addition, the proposed algorithm can be properly verified using the real 3D micro-CT mouse phantom. Experimental reconstruction with a mouse-shaped phantom illustrates the potential of the proposed algorithm.

BLT is an ill-posed inverse source problem, and it is necessary to incorporate sufficient *a priori* information. Currently, five types of *a priori* information are verified and extensively applied in reconstruction algorithms. These include tissue optical parameters, anatomical information, spectral characteristic of source,

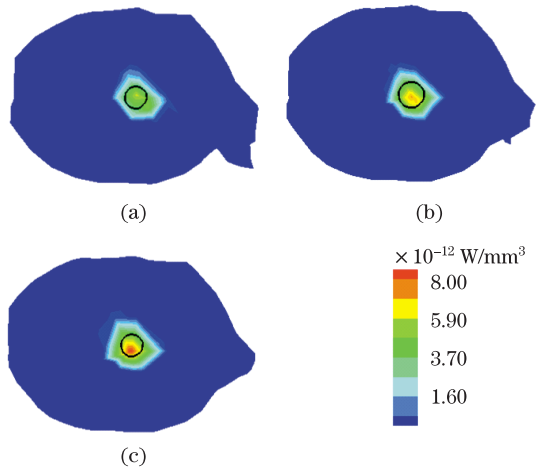


Fig. 5. BLT reconstruction when the source is nearly located at the mouse's center for three different transverse views of the reconstructed results.

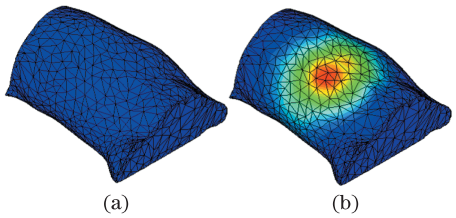


Fig. 6. Mouse-shaped phantom and mapped results. (a) Volumetric mesh used in reconstruction; (b) mapped photon distribution on the phantom.

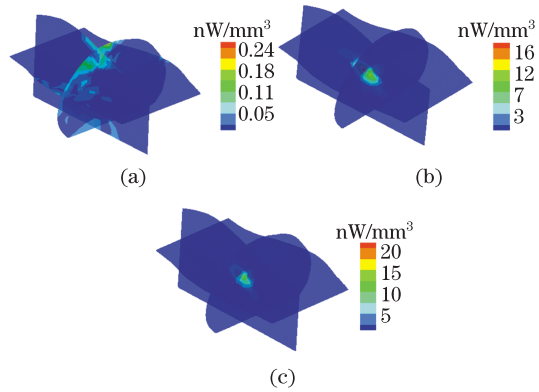


Fig. 7. BLT reconstruction results with the mouse phantom. (a) Reconstruction result with a singleband; (b) BLT reconstruction with the proposed algorithm; (c) reconstructed result with the method of Ref. [9].

distribution of surface photons, and sparsity of source. The five types of *a priori* information are utilized to improve reconstruction quality in our algorithm. To the best of our knowledge, this is the first time that five types of *a priori* information are used to perform BLT reconstruction. Theoretical and instrumentation developments have led to the widespread implementation of multiview noncontact detection and hyper-spectral and multispectral bioluminescence imaging. Therefore, large-scale data and computation burden increase. In our algorithm, the node model of finite element and the optimal permissible source region improve the reconstruction efficiency to a certain extent.

In conclusion, in the sparse Bayesian-based reconstruction algorithm developed for BLT, five types of *a priori* information are used to improve reconstruction. Promising preliminary results are obtained in numerical simulations and experiments, which prove the effectiveness of our proposed algorithm for BLT.

This work was supported by the National Basic Research Program of China (No. 2006CB705700), the National Natural Science Foundation of China (No. 30970780), the Knowledge Innovation Project of the Chinese Academy of Sciences (No. KGCX2-YW-907), the Changjiang Scholars and Innovative Research Team in University (No. IRT0645), the Chinese Academy of Sciences Hundred Talents Program, the Science and Technology Key Project of Beijing Municipal Education Commission (No. KZ200910005005), and the Doctoral Fund of the Ministry of Education of China (No. 20091103110005).

## References

1. B. Chance, Acad. Radiol. **8,** 209 (2001).
2. D. Wang, X. Liu, Y. Chen, and J. Bai, Chin. Opt. Lett. **8,** 82 (2010).
3. B. W. Rice, M. D. Cable, and M. B. Nelson, J. Biomed. Opt. **6,** 432 (2001).
4. G. Wang, Y. Li, and M. Jiang, Med. Phys. **31,** 2289 (2004).
5. A. J. Chaudhari, F. Darvas, J. R. Bading, R. A. Moats, P. S. Conti, D. J. Smith, S. R. Cherry, and R. M. Leahy, Phys. Med. Biol. **50,** 5421 (2005).
6. H. Dehghani, S. C. Davis, S. Jiang, B. W. Pogue, K. D. Paulsen, and M. S. Patterson, Opt. Lett. **31,** 365 (2006).
7. Y. Lv, J. Tian, W. Cong, G. Wang, W. Yang, C. Qin, and M. Xu, Phys. Med. Biol. **52,** 4497 (2007).
8. J. Feng, K. Jia, G. Yan, S. Zhu, C. Qin, Y. Lv, and J. Tian, Opt. Express **16,** 15640 (2008).
9. J. Feng, K. Jia, C. Qin, G. Yan, S. Zhu, X. Zhang, J. Liu, and J. Tian, Opt. Express **17,** 16834 (2009).
10. Y. Lu, X. Zhang, A. Douraghy, D. Stout, J. Tian, T. F. Chan, and A. F. Chatziioannou, Opt. Express **17,** 8062 (2009).
11. L. Jin, Y. Wu, J. Tian, H. Huang, and X. Qu, Chin. Opt. Lett. **7,** 614 (2009).
12. C. Qin, J. Tian, Y. Lv, and W. Yang, Proc. SPIE **6916,** 69161K (2008).
13. J. C. Ye, K. J. Webb, C. A. Bouman, and R. P. Millane. J. Opt. Soc. Am. A **16,** 2400 (1999).
14. A. Genkin, D. D. Lewis, and D. Madigan, Technometrics **49,** 291 (2007).
15. G. Alexandrakis, F. R. Rannou, and A. F. Chatziioannou, Phys. Med. Biol. **50,** 4225 (2005).
16. H. Li, J. Tian, F. Zhu, W. Cong, L. V. Wang, E. A. Hoffman, and G. Wang, Acad. Radiol. **11,** 1029 (2004).
17. C. Kuo, O. Coquoz, T. L. Troy, H. Xu, and B. W. Rice, J. Biomed. Opt. **12,** 024007 (2007).